Fragile-to-strong crossover in optimized In-Sb-Te phase-change supercooled liquids

Yimin Chen,[1,2] Jierong Gu,[2] Qian Zhang,[2] Yuanen Mao,[2] Guoxiang Wang,[2] Rongping Wang,[2,*] Xiang Shen,[2,†] Jun-Qiang Wang,[3,‡] and Tiefeng Xu[2]

[1]*Department of Microelectronic Science and Engineering, School of Physical Science and Technology, Ningbo University, Ningbo, 315211, China*

[2]*Laboratory of Infrared Material and Devices & Key Laboratory of Photoelectric Materials and Devices of Zhejiang Province, Advanced Technology Research Institute, Ningbo University, Ningbo, 315211, China*

[3]*CAS Key Laboratory of Magnetic Materials and Devices & Zhejiang Province Key Laboratory of Magnetic Materials and Application Technology, Ningbo Institute of Materials Technology & Engineering, Chinese Academy of Sciences, Ningbo, 315201, China*

(Received 29 October 2019; revised manuscript received 10 February 2020; accepted 18 February 2020; published 6 March 2020)

We have deposited In-doped Sb_xTe_y ($x:y = 2:3$, 1:1, 3:1, 4:1) phase-change films, and studied their physics properties like crystallization temperature, activation energy, and optical band gap. On the basis of these parameters, a balance between thermal stability and crystallization speed can be found when In content is 20 at. %. We thus further studied their crystallization kinetics using the flash differential scanning calorimetry and the generalized Mauro-Yue-Ellison-Gupta-Allan viscosity model to investigate the potential fragile-to-strong crossover (FSC) in $In_{20}(Sb_2Te_3)_{80}$, $In_{20}(SbTe)_{80}$, $In_{20}(Sb_3Te)_{80}$, and $In_{20}(Sb_4Te)_{80}$ supercooled liquids. It was found that, $In_{20}(Sb_3Te)_{80}$ has a large crossover magnitude (f) of 2.4 with a distinct FSC behavior, but its maximum crystal growth rate (U_{max}) of 0.047 m s^{-1} is too low to satisfy the high-speed phase-change application. The crystal growth rate of In_3SbTe_2 ($In_{51}Sb_{17}Te_{32}$) was found to be 0.08 m s^{-1} without distinct FSC. In contrast, $In_{20}(Sb_4Te)_{80}$ was demonstrated to have a larger U_{max} of 0.425 m s^{-1} and a distinct FSC behavior with a f value of 2.6, which is larger than that of typical phase-change supercooled liquid $Ag_{5.5}In_{6.5}Sb_{59}Te_{29}$. The results strongly support that, obvious FSC is unique only in some phase-change supercooled liquids, but not a universal dynamic feature.

DOI: 10.1103/PhysRevMaterials.4.033403

I. INTRODUCTION

Phase-change memory is considered as a leading candidate for next-generation information storage since it is nonvolatile with fast writing speed, low energy consumption, and high storage density. Digital information is recorded based on the significant difference in electrical resistance and/or optical reflectivity between crystalline and amorphous chalcogenide-based phase-change materials (PCMs) [1]. During the phase-change process, the Joule heating by long low or short high pulses gives rise to crystallization, or melting and subsequent amorphization, respectively [2]. If ignoring the influence of nucleation rate, latent heat of melting and heat capacity, as well as the temperature matching between the PCMs and phase-change device, the maximum crystal growth rate (U_{max}) and melting temperature (T_m) in PCMs mainly determine the writing speed and energy consumption for the phase-change memory cell. Moreover, a good thermal stability with high crystallization temperature, which is usually close to the glass-transition temperature (T_g) in PCMs, is in favor to improve the data storage security. Generally, the smaller T_{gu} ($T_g/T_m - m/505$, m is the supercooled liquid fragility) is, the larger U_{max} is [3]. Therefore, it is a dilemma to have a single material with excellent properties of both high crystal growth rate and good thermal stability.

The addition of various dopants into PCMS is an efficient method to modify the properties of the materials. For example, Sb-Te alloys have a high crystallization rate but a low thermal stability [4]. With the addition of the dopant, the thermal stability can be improved easily, but the crystallization rate would be sacrificed significantly. This has been demonstrated in Ge [5], Si [6], Zn [7], and Ti [8]-doped Sb-Te systems. In addition, the doping of In has been reported to increase the specific temperature and activation energy for crystallization and hinder the crystal growth rate [9]. However, in In-Sb-Te phase-change system, previous reports focused on a pseudobinary alloy along InSb-InTe tie line, like In_3SbTe_2, which has metastable rocksalt structure with Sb and Te randomly disordered on the anion position [10], presenting good thermal stability and fast phase-transition speed [11]. Recently, the compositions out of InSb-InTe tie line have also been discussed, like $In_{15}Sb_{43}Te_{42}$, $In_{24}Sb_{38}Te_{38}$, and $In_{47}Sb_{14}Te_{39}$ films [12]; all of them have high-speed erasing and long-term retention ability. In-doped Sb_2Te [13], Sb_7Te_3 [14], and Sb_4Te [15], were also designed in the applications in phase-change random memory and optical disk.

Most of above investigations focus on the crystallization behavior and thermal stability in phase-change films, but rarely refer crystallization speed, which is expected to

*wangrongping@nbu.edu.cn
†shenxiang@nbu.edu.cn
‡jqwang@nimte.ac.cn

play an important role in data recording process. Understanding the crystallization kinetics is the key to design the fast crystallization speed close to T_m and/or good thermal stability (low crystal growth rate) nearby T_g. By using the method of a novel ultrafast calorimetry, the flash differential scanning calorimetry (DSC) that has a wide heating rate range from 10 to 40 000 K s^{-1}, together with the generalized Mauro-Yue-Ellison-Gupta-Allan (g-MYEGA) viscosity model, Orava *et al.* revealed a fragile-to-strong crossover (FSC) behavior in the supercooled $Ag_{5.5}In_{6.5}Sb_{59}Te_{29}$ (AIST) liquid [16]. Strong FSC behavior present in phase-change supercooled liquids (PCLs) implies that both an ultrahigh crystal-growth rate close to T_m and an ultralow crystal-growth rate near T_g could coexist in a single material, which is an ideal candidate to solve the contradiction between thermal stability and crystallization rate. The crystallization kinetics in other two conventional PCMs, $Ge_2Sb_2Te_5$ [17] and GeTe [18,19], have been investigated by the flash DSC but no distinct FSC behaviors were found in the supercooled liquids. However, the In-Sb-Te phase-change films, such as the pseudobinary $In_3Sb_1Te_2$ and other components that are away from InSb-InTe tie line, are claimed to have both good thermal stability and high crystallization speed, indicating the FSC behavior may present in their supercooled liquids.

The purpose of this paper is to explore crystallization kinetics and FSC behavior in In-Sb-Te phase-change supercooled liquids by the flash DSC and g-MYEGA viscosity model. We first optimized film compositions in In-doped Sb_xTe_y system with high-performance phase-change properties, like the crystallization temperature, the crystallization activation energy, 10-y data retention, and the optical band gap, and then studied the crystallization kinetics to explore the potential FSC behavior in their PCLs. We found that, while FSC can be found in $In_{20}(Sb_3Te)_{80}$ and $In_{20}(Sb_4Te)_{80}$, the absence of FSC in $In_{20}(Sb_2Te_3)_{80}$, $In_{20}(SbTe)_{80}$, and In_3SbTe_2 suggests that FSC is not a universal feature in PCLs.

II. MATERIALS AND METHODS

Amorphous In-doped Sb-Te films were deposited on the substrate of silicon by the magnetron cosputtering method using separated In and Sb_xTe_y ($x : y = 2 : 3$, 1:1, 3:1, 4:1) targets, and $In_{51}Sb_{17}Te_{32}$ (In_3SbTe_2) films were deposited by InSb and InTe targets. In each deposition, the chamber was evacuated to 3×10^{-4} Pa and the working pressure was set at 0.35 Pa. The thickness of the deposited films, which was *in situ* recorded by a thickness monitor equipped in the vacuum chamber and *ex situ* checked by Veeco Dektak 150 surface profiler in air, is about 400 nm. The composition of the films was examined by the energy-dispersive x-ray spectroscopy. The temperature dependent sheet resistance (*R-T*) of the deposited film was measured by the four-probe method with a heating rate of 60 K min^{-1}. The scraped-off flakes from the deposited films were carefully transferred onto UFS-1 chip, and their calorimetric parameters were measured by the Flash DSC from Mettler-Toledo Co. at a heating rate

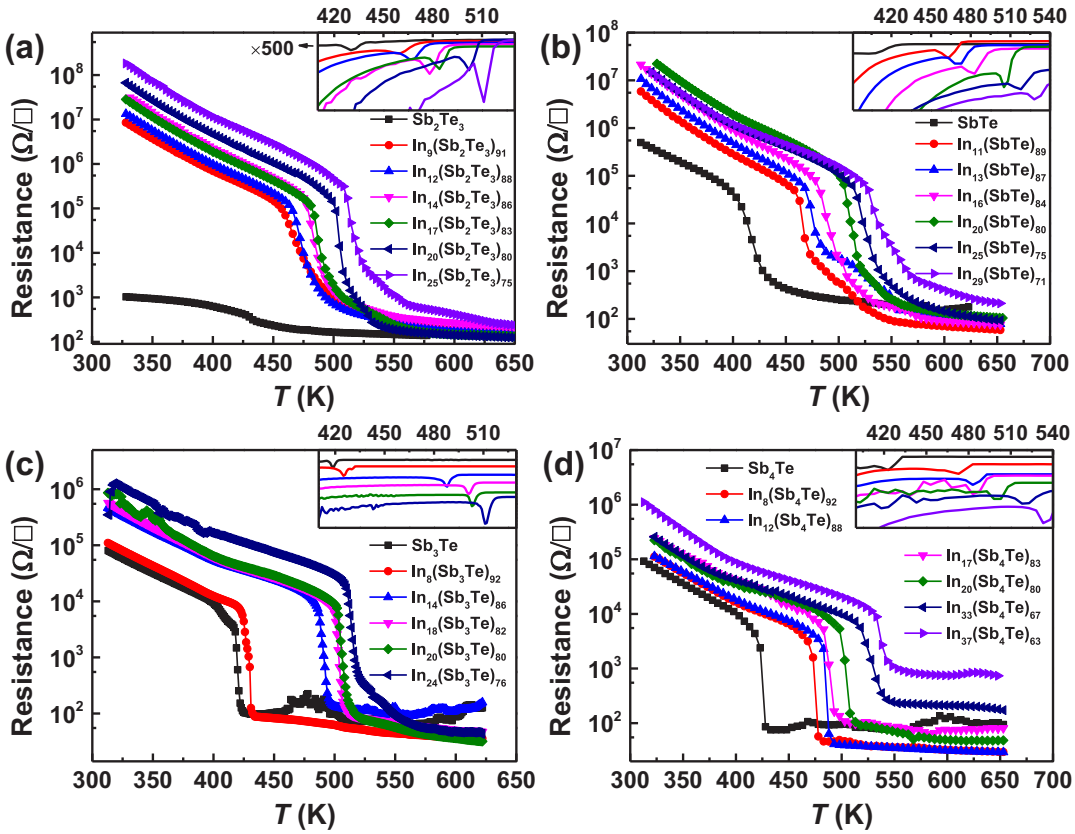

FIG. 1. Temperature dependence of sheet resistance for (a) In-Sb_2Te_3, (b), In-SbTe (c), In-Sb_3Te, and (d) In-Sb_4Te. The heating rate is 60 K min^{-1}. The inset in each figure represents the corresponding differential result (dR/dT). (d) is reproduced from the previous work [21].

range from 20 to 40 000 K s^{-1}. In order to obtain the specific temperature and latent heat for melting, In-Sb-Te bulks were fabricated by melt-quenching method, and about 10 mg material was sealed into an aluminum pan for conventional DSC measurement at a heating rate of 10 K min^{-1}. The Johnson-Mehl-Avrami (JMA) numerical simulation was performed and discussed here to help the study of crystallization kinetics, and a thermal lag issue in the measurement of Flash DSC was also emphasized with a thermal conductivity of amorphous In-Sb-Te from the Supplemental Material of Ref. [10]. See these details in the Supplemental Material [20].

III. RESULTS

A. Screening high-performance materials in In-Sb-Te system

Figures 1(a)–1(d) show the temperature-dependent sheet resistance at a heating rate of 60 K min^{-1} for pure and In-doped Sb_xTe_y ($x:y = 2:3$, 1:1, 3:1, 4:1), respectively. A continuous decrease of the sheet resistance can be found in the heating process for these phase-change films. In each curve, a sharp drop of the sheet resistance at the specific temperature is detected due to the crystallization. The minimum of the first derivative of the temperature-dependent sheet resistance curve is determined as the peak temperature (T_p) for crystallization as shown in the inset in Fig. 1. Obviously, the larger In doping is, the higher T_p is.

Figure 2 shows the activation energy for crystallization (E_a) and the temperature that data can be stored safely for 10 years (T_{10y}) for these films. The latter one is an efficient parameter to evaluate the amorphous thermal stability. E_a and T_{10y} can be extrapolated by fitting the Arrhenius plot of $1/k_BT$ vs failure time t as [22],

$$t = \tau \exp(E_a/k_BT), \tag{1}$$

where τ is a proportional time constant, k_B is the Boltzmann constant. The failure time t is defined as the time when the sheet resistance decreases to its initial value at the specific temperature T. Apparently, the larger In doping is, the higher T_{10y} is. For E_a; however, it decreases slightly for In-doped SbTe and Sb_4Te and is saturated for In-doped Sb_2Te_3 and Sb_3Te films when the In content is more than 20 at. %.

In PCMs, optical band gap E_g is useful to characterize the degree of the disorder. It can be extrapolated from photon

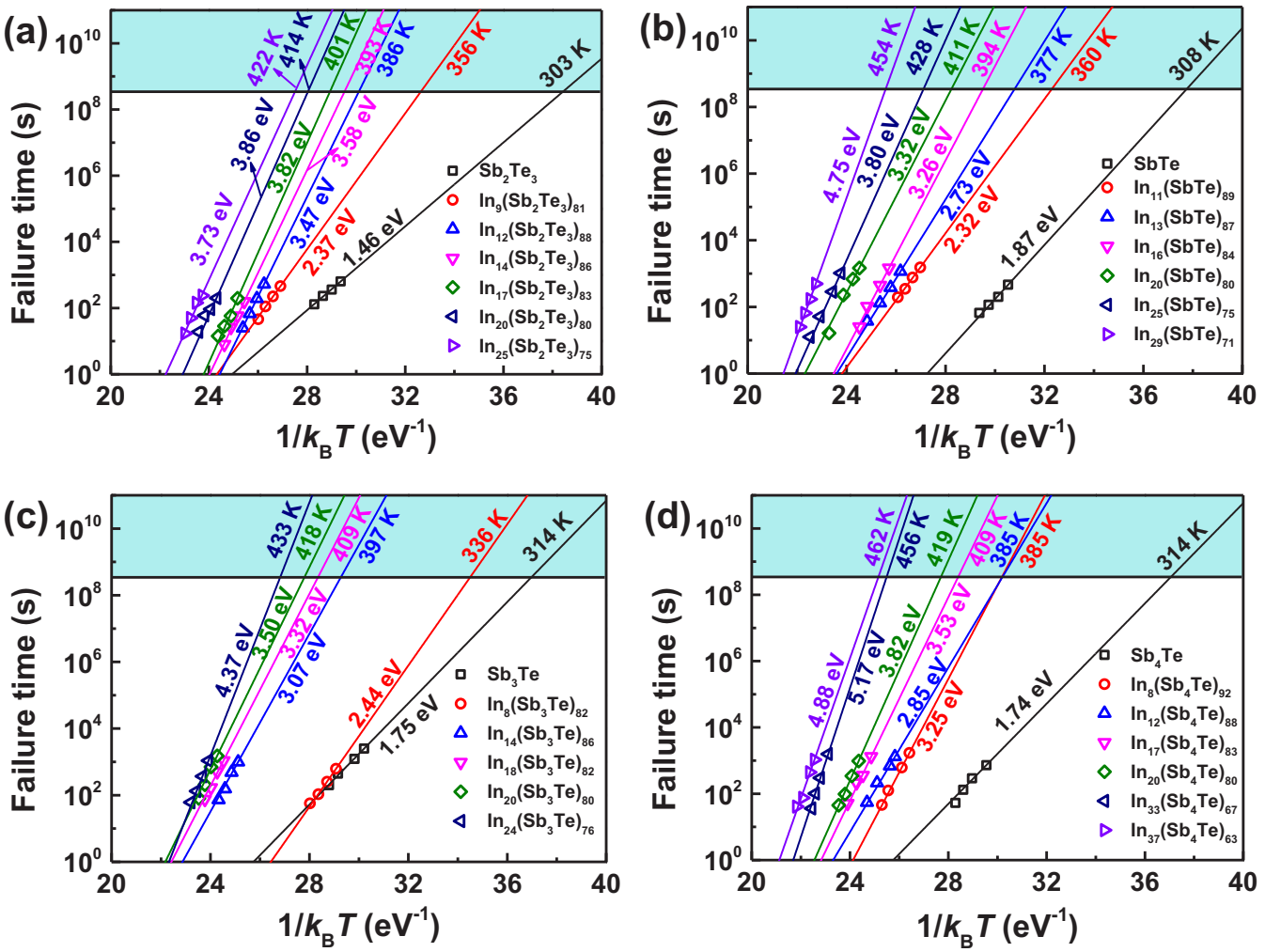

FIG. 2. Activation energy for crystallization and 10-y data retention temperature for (a) In-Sb_2Te_3, (b), In-SbTe (c), In-Sb_3Te, and (d) In-Sb_4Te. (d) is reproduced from previous work [21].

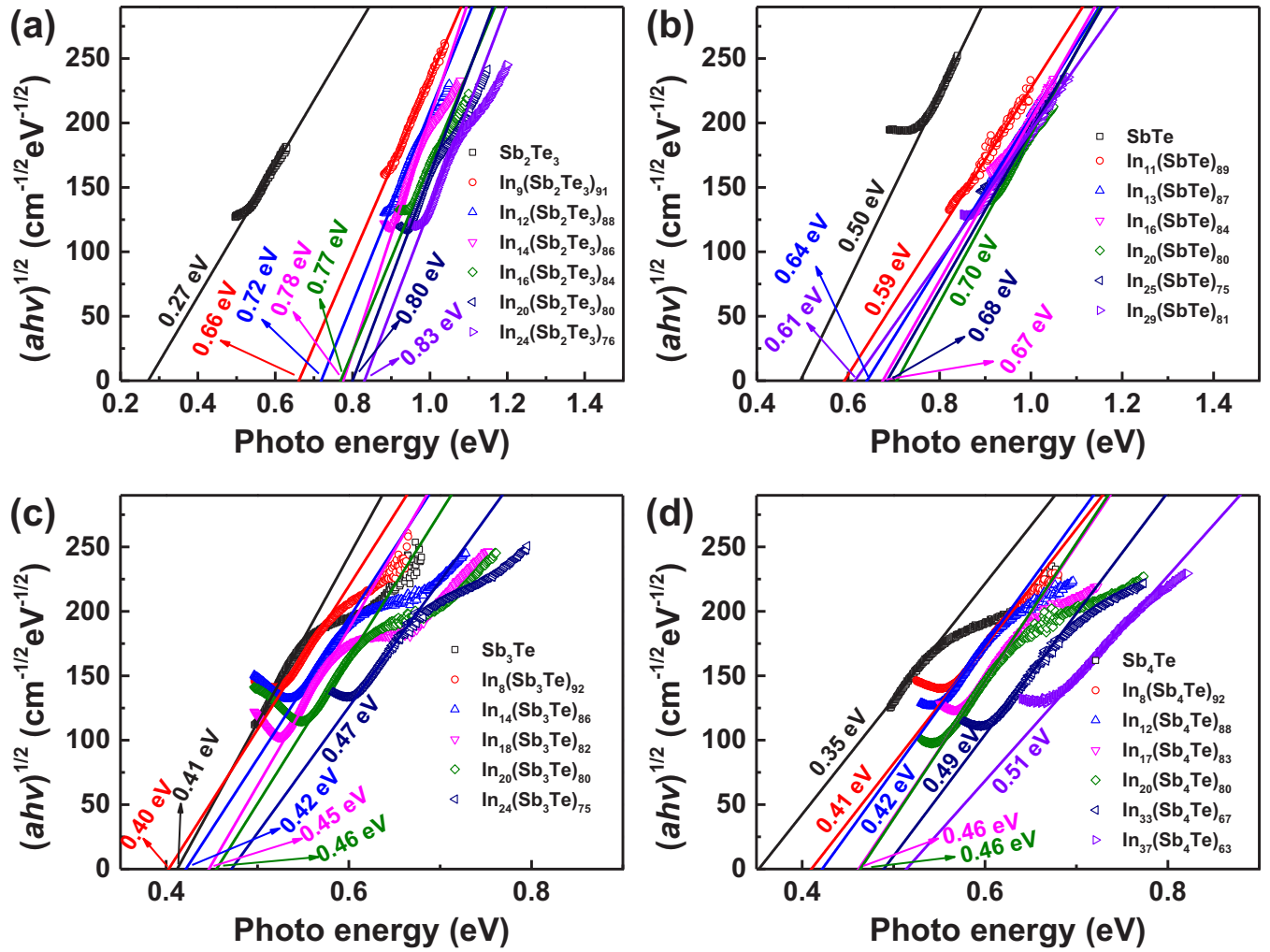

FIG. 3. Tauc plots for (a) In-Sb_2Te_3, (b) In-SbTe, (c) In-Sb_3Te, and (d) In-Sb_4Te, respectively.

energy ($h\nu$)-dependent absorption coefficient (α) by the Tauc plot [23],

$$\alpha h\nu = \beta(h\nu - E_g)^n, \tag{2}$$

where β is the *Tauc* parameter, h is the Planck constant, ν is the frequency, and n is a number depending on the optical transitions, which is $1/2$ for the chalcogenide phase-change film [23]. Figure 3 exhibits the Tauc plots of In-Sb-Te amorphous films and their corresponding E_g values. It is found that E_g increases with increasing In doping up to 20 at. %. With further doping, E_g continues to increase in In-doped Sb_3Te and Sb_4Te, but is changeless in In-doped Sb_2Te_3 and decreases in In-doped SbTe films. Moreover, In-doped Sb_2Te_3 and SbTe films have larger E_g than In-doped Sb_3Te and Sb_4Te, indicating a larger disorder degree. This is in good agreement with the results shown in Fig. 1, i.e., the differences in sheet resistance between amorphous and crystalline state of In-doped Sb_2Te_3, SbTe, Sb_3Te, and Sb_4Te, are 3, 3, 5, and 5 orders of magnitudes, respectively.

All the characteristic parameters including T_p, E_a, T_{10y}, and E_g for In-doped Sb_xTe_y films are presented in Fig. 4. As we know, the higher T_p and T_{10y} and the larger E_a are a benefit to improve amorphous thermal stability, and the larger E_g is necessary to obtain higher ratio of signal to noise. According to the results shown in Fig. 4, it can be concluded that, the larger In doping is, the higher T_p, T_{10y}, and larger E_a, E_g are. Although the thermal stability and ratio of signal to noise improve obviously, the phase-transition speed or the crystallization rate would be sacrificed significantly with increasing dopant. Nevertheless, such parameters appear to reach a maximum value in In-Sb_xTe_y films with In content of 20 at. %, implying that a balance between good thermal stability and high crystallization speed might be achieved. In our previous work [24], E_a and T_{10y} were extrapolated by strict Arrhenius behavior to evaluate the thermal stability, and then the optimal dopant content of Zn in Sb-Te alloys for high-performance PCMs was determined to be ~30 at. %. However, the low scanning rate with narrow test temperature range could result in a pseudo-Arrhenius behavior. The experiments performed at fast scanning rate with a broad range of temperature are suitable to investigate the crystallization kinetics in the supercooled liquids. In terms of this, flash DSC that can provide the ultrafast scanning rate more than 40 000 K s^{-1} could be a powerful tool.

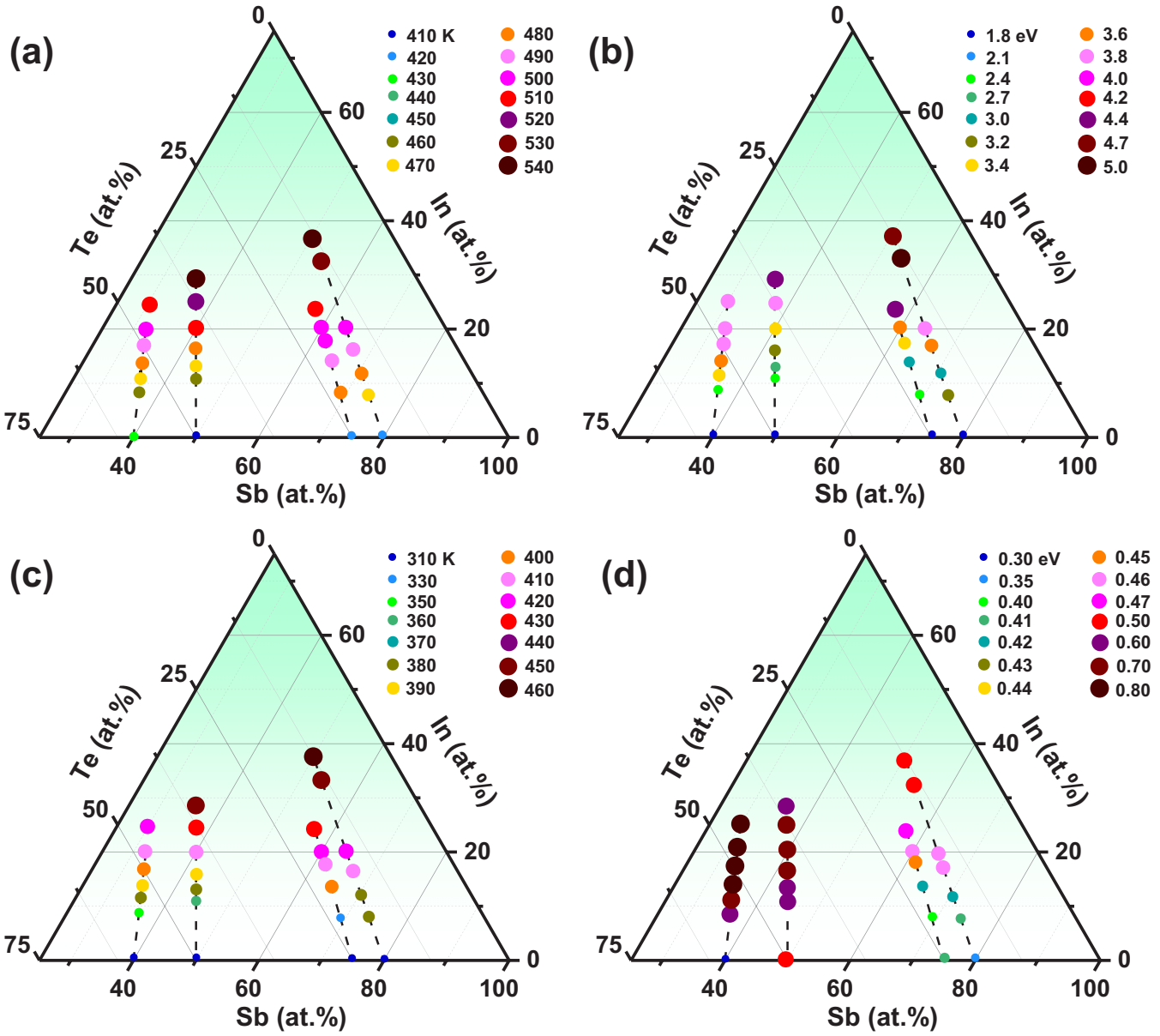

FIG. 4. The diagrams related to (a) T_p, (b) E_a, (c) $T_{10\,y}$, and (d) E_g, for In-doped Sb_xTe_y ($x : y = 2 : 3$, 1:1, 3:1, 4:1) films. The color and corresponding size of each dot represents the specific value, which is classified by different range. The classification is drawn out at upper right in each diagram.

B. Fragile-to-strong crossover of In-Sb-Te supercooled liquids

Recently, the flash DSC has been used to study the crystallization kinetics of PCLs, giving the information like thermal stability and crystallization speed. For example, $Ge_2Sb_2Te_5$ (GST) and GeTe were demonstrated to have large fragility with fast crystallization rate; AIST was confirmed to have FSC behavior that can solve a dilemma between thermal stability and crystallization speed.

Although the study of the crystallization kinetics of $In-Sb_4Te$ films using flash DSC has been reported, the bad fitting quality and inadequate analysis based on Mauro-Yue-Ellison-Gupta-Allan (MYEGA) viscosity model lead to an ambiguous result that no FSC behavior exists in such PCLs [21]. We here employed the g-MYEGA viscosity model to investigate the possible FSC behavior in In-Sb-Te PCLs. Flash DSC traces of $In_{20}(Sb_xTe_y)_{80}$ are shown in Fig. 5. The peak temperature for crystallization T_p with a strong exothermic signal can be found in each heating trace. It becomes higher when the heating rate is faster. These data are all performed in Fig. 6 as the Kissinger plot in the form of $1000/T_p$ vs $\ln(\phi/T_p^2)$ for crystallization [25],

$$\ln\left(\phi/T_p^2\right) = -Q/RT_p + A, \tag{3}$$

where ϕ is heating rate, Q is the activation energy for crystallization, R is the gas constant as $8.314\,J(mol\cdot K)^{-1}$, and A is a constant. From T_p values obtained from flash DSC and R-T measurements, it is found that, the activation energy Q becomes curved and decreases with increasing heating rate,

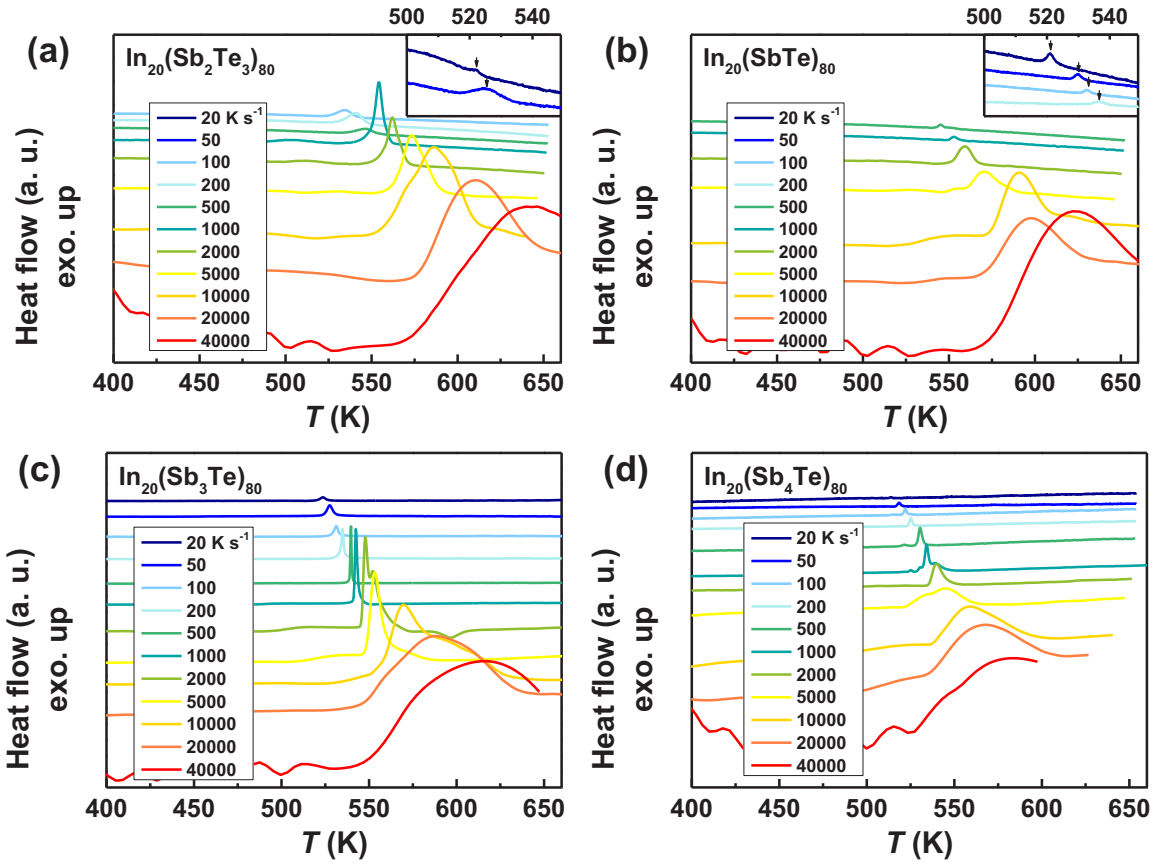

FIG. 5. Flash DSC traces for (a) $In_{20}(Sb_2Te_3)_{80}$, (b) $In_{20}(SbTe)_{80}$, (c) $In_{20}(Sb_3Te)_{80}$, and (d) $In_{20}(Sb_4Te)_{80}$ films. The heating rate is in the range of 20 to 40 000 K s^{-1}. (d) is reproduced from previous work [21].

implying a strong non-Arrhenius behavior in the In-Sb-Te PCLs.

Henderson confirmed that [26] the Kissinger method can be used for crystallization kinetics study when the temperature T_p is equal to $T_{0.63}$ (the temperature at which crystallized fraction is 0.63). This was also emphasized recently by Orava and Greer [27], who claimed that the unreliable threshold of the heating rate for the Kissinger method used to estimate an approximation of crystal growth rate is 10 000 K s^{-1} for the phase-change material $Ge_2Sb_2Te_5$. Here, the JMA numerical simulated DSC traces with heating rates from 20 to 40 000 K s^{-1} and the corresponding crystallized fraction of these In-doped Sb-Te PCLs are studied (see the details in Fig. S3 and Table S1 of Supplemental Material [20]). It was found that, the difference between T_p and $T_{0.63}$ is presented more or less in $In_{20}(Sb_2Te_3)_{80}$, $In_{20}(SbTe)_{80}$, $In_{20}(Sb_3Te)_{80}$ (as well as In_3SbTe_2 that will be discussed later) when the heating rate ϕ is more than 5000 K s^{-1}, indicating the Kissinger plots of these PCLs (see Fig. 6) could not be considered as the crystallization kinetics coefficient U_{kin} directly. However, by the help of JMA numerical simulation, the true temperature-dependent U_{kin} can also be obtained. For $In_{20}(Sb_4Te)_{80}$, there is no obvious difference between T_p and $T_{0.63}$ even at a heating rate of 40 000 K s^{-1}, implying the Kissinger plot can be considered as U_{kin} directly.

On the basis of Stokes-Einstein relation of $U_{kin} \propto \eta^{-1}$ that describes the relationship between viscosity η and U_{kin} [28], the logarithmic scale of U_{kin} can be expressed as

$$\log_{10} U_{kin} = C - \log_{10}\eta, \tag{4}$$

where C is a constant to illustrate the difference between U_{kin} and η^{-1}. Here, we used g-MYEGA viscosity model to describe the temperature-dependent viscosity η of In-Sb-Te PCLs. The equation for g-MYEGA viscosity model is [29]

$$\log_{10}\eta = \log_{10}\eta_\infty + \frac{1}{T\left[W_1 \exp\left(-\frac{C_1}{T}\right) + W_2 \exp\left(-\frac{C_2}{T}\right)\right]}, \tag{5}$$

where η_∞ is the viscosity at infinite high temperature, W_1 and W_2 are the weight coefficients to describe the brittle and the strong item, respectively. C_1 and C_2 are the two constraint starting temperature constants corresponding to the two mechanisms of brittleness and strength, respectively. Together with Eqs. 4 and 5, U_{kin} can be expressed as,

$$\log_{10} U_{kin} = C - \log_{10}\eta_\infty - \frac{1}{T\left[W_1 \exp\left(-\frac{C_1}{T}\right) + W_2 \exp\left(-\frac{C_2}{T}\right)\right]}. \tag{6}$$

Together with the T_p data from flash DSC measurement and the JMA numerical simulation at higher heating rate, the

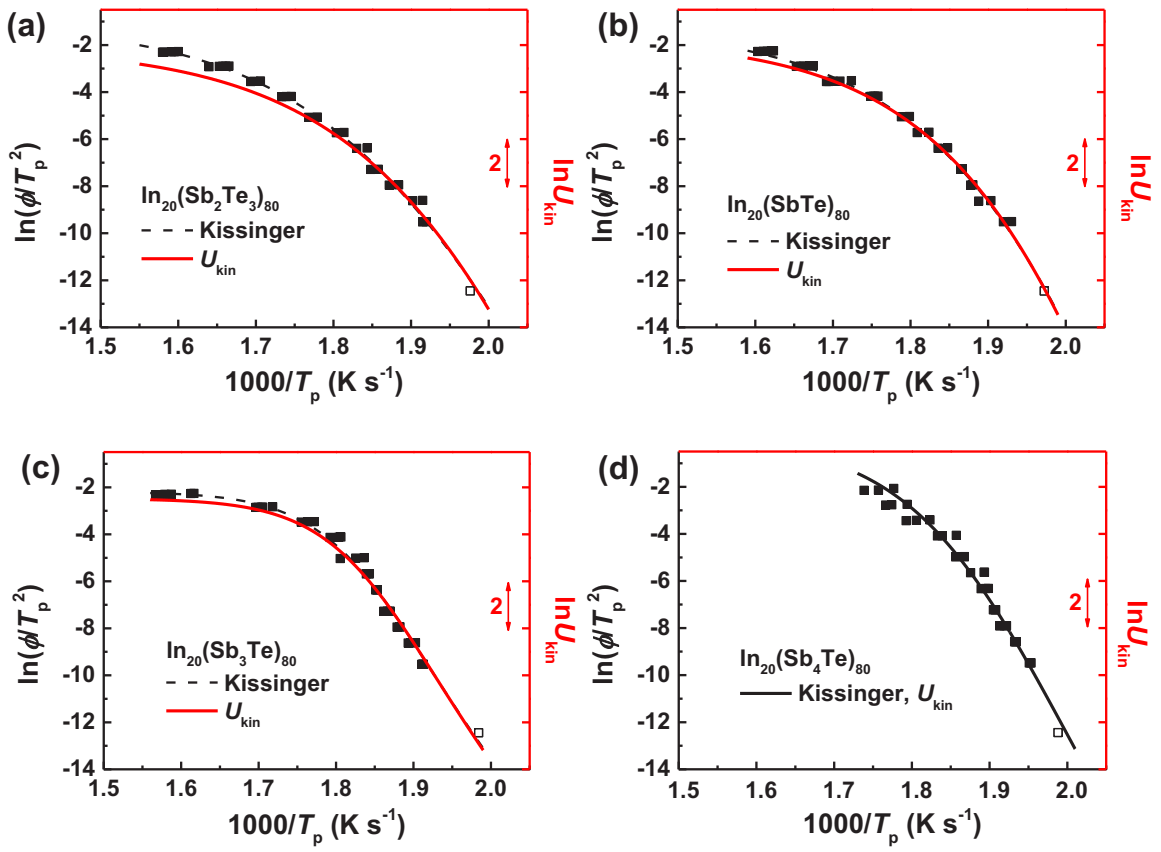

FIG. 6. Kissinger plots and the corresponding crystallization kinetics coefficient U_{kin} of (a) $In_{20}(Sb_2Te_3)_{80}$, (b) $In_{20}(SbTe)_{80}$, (c) $In_{20}(Sb_3Te)_{80}$, and (d) $In_{20}(Sb_4Te)_{80}$. The dashed curves are the Kissinger plots and the solid curves are the U_{kin} which are fitted by using the g-MYEGA viscosity model. The solid and open symbols represent the values of T_p obtained from flash DSC and *R-T* test, respectively.

temperature-dependent U_{kin} of In-Sb-Te PCLs can be extrapolated and the results are also shown in Fig. 6 as depicted in solid curves. The corresponding fitting parameters are listed in Table I. The crossover temperature T_{f-s} can be estimated as [30]

$$T_{f-s} = \frac{C_1 - C_2}{\ln W_1 - \ln W_2}. \tag{7}$$

Such temperatures for In-Sb-Te PCLs are also listed in Table I.

Figure 7 shows the Angell plots for In-Sb-Te PCLs. The thick curves represent the transposed ${U_{kin}}^{-1}$, and the thin ones indicate the temperature-dependent viscosity, which is extrapolated by the g-MYEGA viscosity model. It is important to know the exact value of T_g for transposing the data onto viscosity plots and deriving the fragility index as

$$m = \frac{d\log_{10}\eta}{d(T_g/T)}. \tag{8}$$

Depending on the standard viscosity of 10^{12} Pa s at T_g, we defined the T_g as 435, 445, 406, and 408 K, for $In_{20}(Sb_2Te_3)_{80}$, $In_{20}(SbTe)_{80}$, $In_{20}(Sb_3Te)_{80}$, and $In_{20}(Sb_4Te)_{80}$, respectively. We note there could be no decoupling in these PCLs with the FSC behavior, because the fragile liquid does not persist to low temperature [16].

From the Angell plots, we can see that a distinct FSC behavior exhibits in $In_{20}(Sb_3Te)_{80}$ and $In_{20}(Sb_4Te)_{80}$ PCLs, but such a behavior becomes weak in $In_{20}(Sb_2Te_3)_{80}$ and $In_{20}(SbTe)_{80}$. In order to get insight into the FSC behavior, we employed the MYEGA viscosity model to independently

TABLE I. The fitting parameters estimated from temperature-dependent U_{kin} by g-MYEGA viscosity model, as well as the T_{f-s}, fragility m, m', and the crossover magnitude f.

PCLs	η_∞(Pa s)	W_1	W_2	C_1	C_2	T_{f-s} (K)	m	m'	f
$In_{20}(Sb_2Te_3)_{80}$	$10^{-2.99}$	85	7.25×10^{-4}	6 334	812	473	95	114	1.2
$In_{20}(SbTe)_{80}$	$10^{-3.06}$	204	1×10^{-4}	6 757	20	445	99	153	1.5
$In_{20}(Sb_3Te)_{80}$	$10^{-3.01}$	5.8×10^{9}	0.01	16 107	1673	533	77	188	2.4
$In_{20}(Sb_4Te)_{80}$	$10^{-3.00}$	251 740	0.0012	10 690	816	517	86	222	2.6

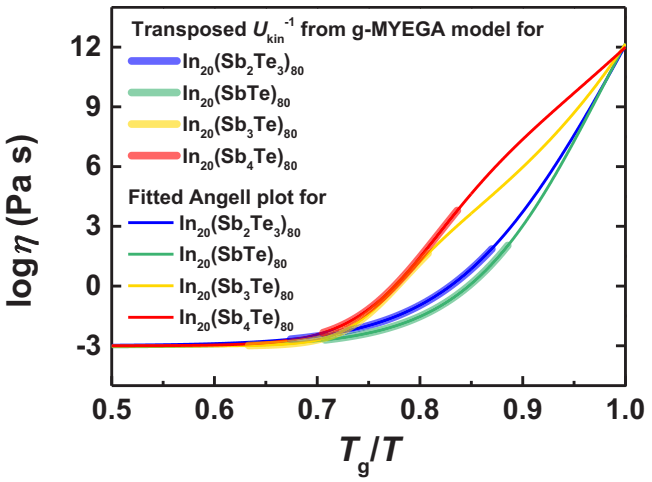

FIG. 7. Angell plots for In-Sb-Te PCLs, which are fitted by the viscosity model of g-MYEGA. The thick curves are the transposed $U_{kin}{}^{-1}$ from g-MYEGA viscosity model.

describe the temperature-dependent viscosity in strong and fragile liquids. The MYEGA viscosity model can be written as [31]

$$\log_{10}\eta = \log_{10}\eta_\infty + \frac{B}{T}\exp\left(\frac{C}{T}\right), \tag{9}$$

where η_∞ is the viscosity at infinite high temperature, B and C are constants, both of which are related to the onset of rigidity in the supercooled liquid. With the best fitting, fragility index m and m' for strong and fragile liquid can be estimated by Eq. (8) at the temperature $T = T_g$ and $T = T_{f-s}$, respectively. Such fitting process is shown in Fig. S5 of Supplemental Material for In_3SbTe_2 as an example [20]. The values of m and m', as well as the crossover magnitude f that is defined as m'/m, are all listed in Table I. $In_{20}(Sb_2Te_3)_{80}$, $In_{20}(SbTe)_{80}$, $In_{20}(Sb_3Te)_{80}$, and $In_{20}(Sb_4Te)_{80}$ PCLs have the f value of 1.2, 1.5, 2.4, 2.6, with the T_{f-s} of 473, 445, 533, 517 K, respectively.

Following previous works [19,25,28], we estimated the temperature-dependent crystal growth rate U by the expression [32]

$$U = U_{kin}[1 - \exp(-\Delta G/RT)], \tag{10}$$

where U_{kin} is the crystallization kinetics coefficient that has been obtained from the Kissinger plot, and ΔG is the driving force for crystallization. For chalcogenide supercooled liquids, their ΔG should obey the formula suggested by Thompson and Spaepen, which is [33]

$$\Delta G = \frac{\Delta H_m \Delta T}{T_m}\left(\frac{2T}{T_m + T}\right), \tag{11}$$

where $\Delta T\,(T_m - T)$ is the undercooling temperature, T_m is the melting temperature, and ΔH_m is the latent heat for melting. The values of T_m and ΔH_m for $In_{20}(Sb_2Te_3)_{80}$, $In_{20}(SbTe)_{80}$, $In_{20}(Sb_3Te)_{80}$, and $In_{20}(Sb_4Te)_{80}$, can be obtained from the conventional DSC traces as shown in Fig. 8(a), and the results are 890, 819, 832, 829 K, and 15.7, 19.1, 23.5, 18.2 kJ mol^{-1}, respectively. Taking the fitting parameters listed in Table I into Eq. (10), the reduced temperature-dependent U can be extrapolated as shown in Fig. 8(b). We found they have the maximum crystal growth rate U_{max} of 0.002, 0.05, 0.035, 0.31 m s^{-1} at the corresponding reduced temperature T_{max}/T_m of 0.822, 0.788, 0.752, 0.785, respectively.

IV. DISCUSSION

The concept of FSC was first proposed for water by Angell [34], and later found in liquid SiO_2 [35] and BF_2 [36], as well as the metallic glasses like Cu-Zr-Al [30]. For chalcogenides, it was confirmed that supercooled liquids $Ge_{30}Se_{70}$ [37] and $Ge_{15}Te_{85}$ [38] have distinct FSC behavior. The conventional chalcogenide PCM, AIST, was also revealed to have FSC by studying its crystallization kinetics [16]. It is believed that finding materials with large crossover magnitude f is a way to solve the contradiction between fast crystallization close to T_m and good thermal stability nearby T_g in PCMs. Thus, we optimized the PCMs in In-Sb-Te system and investigated their crystallization kinetics with FSC behavior. Together with

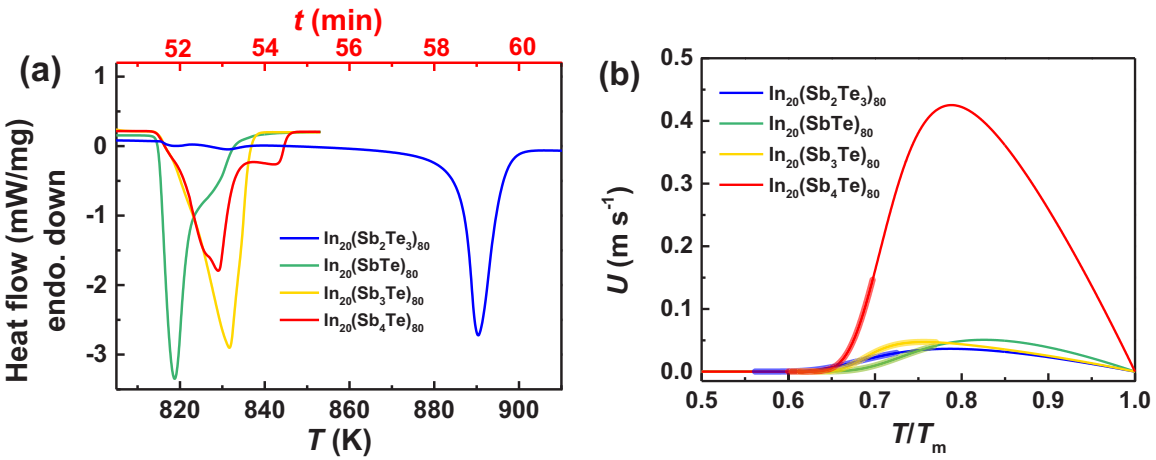

FIG. 8. (a) Conventional DSC traces of In-Sb-Te alloys. The heating rate is 10 K min^{-1}. (b) Temperature-dependent crystal growth rate U for In-Sb-Te PCLs. The thick and thin curves are the transposed and extrapolated results, respectively.

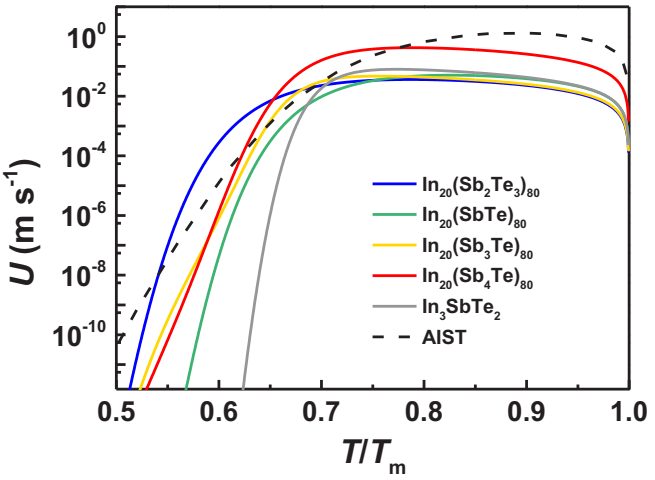

FIG. 9. The logarithmic scale of temperature-dependent U for In-Sb-Te. The dashed line represents the temperature dependent U of AIST that was carried out by Orava *et al.* [17].

flash DSC and g-MYEGA viscosity model, we found that $In_{20}(Sb_3Te)_{80}$ has a large f value of 2.4 with distinct FSC behavior, but its low U_{max} might hinder it to be a candidate for high-speed memory storage. $In_{20}(Sb_2Te_3)_{80}$ and $In_{20}(SbTe)_{80}$ with small f values and low U_{max} are suggested unsuitable for phase-change memory too. $In_{20}(Sb_4Te)_{80}$ was revealed to have both large f value of 2.6 and fast crystal-growth rate U_{max} of 0.425 m s^{-1}. As redrawn in Fig. 9, we knew the value of U_{max} is about 1 m s^{-1} for AIST, which is three times larger than that of $In_{20}(Sb_4Te)_{80}$. However, compared to AIST, the larger f value makes it possible to be a PCM for high-temperature memory storage. It should be noted that the crystallization kinetics of In_3SbTe_2, which is the most famous in In-Sb-Te system with a metastable rocksalt structure like GST [10], was also studied using the same method and model (see the details in the Supplemental Material [20]). We found that In_3SbTe_2 almost has no FSC behavior with very small f and U_{max} of 1.1 and 0.08 m s^{-1}, respectively (see the T_m and ΔH_m in Fig. S6 of the Supplemental Material of Ref. [39]) Therefore, it is reasonable to conclude that $In_{20}(Sb_4Te)_{80}$ material can be the best one for high-performance memory storage in In-Sb-Te system.

Three issues may be the most important that need to be solved in the FSC behavior in PCLs. The first is the mechanism of FSC in PCLs. The competition among medium-range ordering (MRO) clusters composed of different configurations of the locally ordered structural units was claimed for FSC in Cu-Al and Cu-Zr-Al metallic glass-forming liquids [30,40]. Wei *et al.* proposed that FSC in $Ge_{15}Te_{85}$ liquid is not only related to structural changes in MRO clusters, but also associated with the rate of expansion of short-range ordering (SRO) [41]. Very recently, Zalden *et al.* associated the liquid-liquid transition with Peierls distortion that accounts for the FSC in $Ge_{15}Sb_{85}$ and AIST liquids [42]. It is unclear whether Peierls distortion, SRO, and/or MRO clusters can be as the sole or mixed structural origin for FSC behavior. The second is the FSC behavior in confined PCLs. It has been reported that GST and GeTe have no distinct FSC in their supercooled liquids [18,19], but the obvious FSC behaviors are observed in confined nanoparticle (zero-dimension) GST [43] and GeTe [44]. Hence, it is interesting to search the FSC behaviors in other confined PCLs, such as ultrathin films (two dimension), nanowires (one dimension). The third is the universality of FSC in PCLs. Mallamace *et al.* emphasized that the FSC behavior has a larger generality than the traditional Angell classification of liquids into two separate classes of glass formers: fragile and strong [45]. Zhang *et al.* suggested the FSC might be a universal dynamic feature in all metallic glass-forming liquids from the data of the temperature-dependent viscosity for many metallic glasses [29]. Orava *et al.* also proposed such universal feature presents in PCLs, but no more evidences to support this point [17]. The study of FSC crystallization kinetics of In-Sb-Te in this work shows that the distinct FSC exists in $In_{20}(Sb_4Te)_{80}$ and $In_{20}(Sb_3Te)_{80}$, but this is absent in $In_{20}(Sb_2Te_3)_{80}$, $In_{20}(SbTe)_{80}$, and In_3SbTe_2 supercooled liquids. It seems to indicate that FSC behavior is not a universal dynamic feature in PCLs, but further investigation is still needed.

V. CONCLUSIONS

In this work, the phase-change characters and crystallization kinetics of In-Sb-Te films have been investigated. We found that, when the content of In doping is 20 at. % in In-Sb_xTe_y ($x:y = 2:3$, 1:1, 3:1, 4:1), the films show high crystallization temperature and activation energy for long-term memory storage, and large optical band gap for safe memory storage. The crystallization kinetics and FSC behavior were studied by flash DSC and g-MYEGA viscosity model. It was found that the optimized $In_{20}(Sb_2Te_3)_{80}$, $In_{20}(SbTe)_{80}$, $In_{20}(Sb_3Te)_{80}$, $In_{20}(Sb_4Te)_{80}$, and In_3SbTe_2 has the U_{max} of 0.036, 0.051, 0.047, 0.425, and 0.08 m s^{-1}, at the corresponding reduced temperature T_{max}/T_m of 0.787, 0.7826, 0.756, 0.786, and 0.774, respectively. Among them, $In_{20}(Sb_3Te)_{80}$ and $In_{20}(Sb_4Te)_{80}$ exhibit distinct FSC behavior with a crossover magnitude f of 2.4 and 2.6, at the specific temperature T_{f-s} is 533 and 517 K, respectively. Therefore, $In_{20}(Sb_4Te)_{80}$ film with a fast crystal growth rate and a large crossover magnitude can be the best one for potential applications in high-performance memory storage. Moreover, the obvious FSC is unique only in some of the phase-change supercooled liquids, and this seems to indicate that the FSC is not a universal dynamic feature.

ACKNOWLEDGMENTS

The project is supported by the Natural Science Foundation of China (Grants No. 61775111, No. 61775109, No. 51771216, and No. 61904091), Zhejiang Provincial Natural Science Foundation of China (Grant No. LR18E010002), the Natural Science Foundation of Ningbo City, China (Grant No. 2019A610065), the International Cooperation Project of Ningbo City (Grant No. 2017D10009), National Key R&D Program of China (Grant No. 2018YFA0703604), 3315 Innovation Team in Ningbo City, and sponsored by K. C. Wong Magna Fund in Ningbo University, China.

[1] F. Rao, K. Ding, Y. Zhou, Y. Zheng, M. Xia, S. Lv, Z. Song, and S. Feng, Science **358**, 1423 (2017).

[2] M. Wuttig and N. Yamada, Nat. Mater. **6**, 824 (2007).

[3] J. Orava and A. Greer, J. Chem. Phys. **140**, 214504 (2014).

[4] M. H. R. Lankhorst, L. v. Pieterson, M. v. Schijndel, B. A. J. Jacobs, and J. C. N. Rijpers, J. Appl. Phys. **42**, 863 (2003).

[5] P. K. Khulbe, T. Hurst, M. Horie, and M. Mansuripur, Appl. Opt. **41**, 6220 (2002).

[6] Y. Zhang, J. Feng, Z. Zhang, B. Cai, Y. Lin, T. Tang, and B. Chen, Appl. Surf. Sci. **254**, 5602 (2008).

[7] X. Shen, G. Wang, R. P. Wang, S. Dai, L. Wu, Y. Chen, T. Xu, and Q. Nie, Appl. Phys. Lett. **102**, 131902 (2013).

[8] M. Zhu, L. Wu, F. Rao, Z. Song, K. Ren, X. Ji, S. Song, D. Yao, and S. Feng, Appl. Phys. Lett. **104**, 053119 (2014).

[9] H. T. Nguyen, A. Kusiak, J. L. Battaglia, C. Gaborieau, Y. Anguy, R. Fallica, C. Wiemer, A. Lamperti, and M. Longo, Adv. Sci. Technol. **95**, 113 (2014).

[10] T. Schröder, T. Rosenthal, S. Grott, C. Stiewe, J. de Boor, and O. Oeckler, Z. Anorg. Allg. Chem. **639**, 2536 (2013).

[11] E. T. Kim, J. Y. Lee, and Y. T. Kim, Phys. Status Solidi-R. **3**, 103 (2009).

[12] L. Men, F. Jiang, and F. Gan, Mater. Sci. Eng. B **47**, 18 (1997).

[13] L. Hromádko, J. Přikryl, L. Střižík, P. Košťál, L. Beneš, and M. Frumar, J. Alloys Compd. **617**, 306 (2014).

[14] Y. S. Hsu, Y. C. Her, S. T. Cheng, and S. Y. Tsai, IEEE Trans. Magn. **43**, 937 (2007).

[15] S. Selmo, S. Cecchi, R. Cecchini, C. Wiemer, M. Fanciulli, E. Rotunno, L. Lazzarini, and M. Longo, Phys. Status Solidi A **213**, 335 (2016).

[16] J. Orava, D. W. Hewak, and A. L. Greer, Adv. Funct. Mater. **25**, 4851 (2015).

[17] J. Orava, A. L. Greer, B. Gholipour, D. W. Hewak, and C. E. Smith, Nat. Mater. **11**, 279 (2012).

[18] H. Weber, J. Orava, I. Kaban, J. Pries, and A. L. Greer, Phys. Rev. Mater. **2**, 093405 (2018).

[19] Y. Chen, G. Wang, L. Song, X. Shen, J. Wang, J. Huo, R. Wang, T. Xu, S. Dai, and Q. Nie, Cryst. Growth Des. **17**, 3687 (2017).

[20] See Supplemental Material at http://link.aps.org/supplemental/10.1103/PhysRevMaterials.4.033403 for the thermal lag issue in the measurement of Flash DSC, the Johnson-Mehl-Avrami numerical simulations, the validity of Kissinger method for In-Sb-Te crystallization kinetics study, and the crystallization kinetics of In_3SbTe_2.

[21] S. Mu, Y. Chen, H. Pan, G. Wang, J. Wang, R. Wang, X. Shen, S. Dai, T. Xu, and Q. Nie, CrystEngComm **20**, 159 (2018).

[22] Y. Chen, G. Wang, X. Shen, T. Xu, R. P. Wang, L. Wu, Y. Lu, J. Li, S. Dai, and Q. Nie, CrystEngComm **16**, 757 (2014).

[23] K. D. Shukla, S. Sahu, A. Manivannan, and U. P. Deshpande, Phys. Status Solidi-R. **11**, 1700273 (2017).

[24] G. Wang, Y. Chen, X. Shen, Y. Lu, S. Dai, Q. Nie, and T. Xu, J. Appl. Phys. **117**, 045303 (2015).

[25] Y. Chen, H. Pan, S. Mu, G. Wang, R. Wang, X. Shen, J. Wang, S. Dai, and T. Xu, Acta Mater. **164**, 473 (2019).

[26] D. W. Henderson, J. Non-Cryst. Solids **30**, 301 (1979).

[27] J. Orava and A. L. Greer, Thermochim. Acta **603**, 63 (2015).

[28] Y. Chen, R. Wang, X. Shen, J. Wang, and T. Xu, Cryst. Growth Des. **19**, 1103 (2019).

[29] C. Zhang, L. Hu, Y. Yue, and J. C. Mauro, J. Chem. Phys. **133**, 014508 (2010).

[30] C. Zhou, L. Hu, Q. Sun, H. Zheng, C. Zhang, and Y. Yue, J. Chem. Phys. **142**, 064508 (2015).

[31] J. C. Mauro, Y. Yue, A. J. Ellison, P. K. Gupta, and D. C. Allan, Proc. Natl. Acad. Sci. USA **106**, 19780 (2009).

[32] M. Ediger, P. Harrowell, and L. Yu, J. Chem. Phys. **128**, 034709 (2008).

[33] C. V. Thompson and F. Spaepen, Acta Metall. **27**, 1855 (1979).

[34] C. A. Angell, J. Chem. Phys. B **97**, 6339 (1993).

[35] I. Saika-Voivod, P. H. Poole, and F. Sciortino, Nature (London) **412**, 514 (2001).

[36] M. Hemmati, C. T. Moynihan, and C. A. Angell, J. Chem. Phys. **115**, 6663 (2001).

[37] S. Stølen, T. Grande, and H. B. Johnsen, Phys. Chem. Chem. Phys. **4**, 3396 (2002).

[38] S. Wei, P. Lucas, and C. A. Angell, J. Appl. Phys. **118**, 034903 (2015).

[39] V. Bilovol and B. Arcondo, J. Non Cryst. Solids **447**, 315 (2016).

[40] J. Kang, J. Zhu, S.-H. Wei, E. Schwegler, and Y.-H. Kim, Phys. Rev. Lett. **108**, 115901 (2012).

[41] S. Wei, M. Stolpe, O. Gross, W. Hembree, S. Hechler, J. Bednarcik, R. Busch, and P. Lucas, Acta Mater. **129**, 259 (2017).

[42] P. Zalden, F. Quirin, M. Schumacher, J. Siegel, S. Wei, A. Koc, M. Nicoul, M. Trigo, P. Andreasson, H. Enquist, M. J. Shu, T. Pardini, M. Chollet, D. Zhu, H. Lemke, I. Ronneberger, J. Larsson, A. M. Lindenberg, H. E. Fischer, S. Hau-Riege, D. A. Reis, R. Mazzarello, M. Wuttig, and K. Sokolowski-Tinten, Science **364**, 1062 (2019).

[43] B. Chen, G. H. ten Brink, G. Palasantzas, and B. J. Kooi, J. Chem. Phys. C **121**, 8569 (2017).

[44] B. Chen, D. de Wal, G. H. Ten Brink, G. Palasantzas, and B. J. Kooi, Cryst. Growth Des. **18**, 1041 (2018).

[45] F. Mallamace, C. Branca, C. Corsaro, N. Leone, J. Spooren, S. H. Chen, and H. E. Stanley, Proc. Natl. Acad. Sci. USA **107**, 22457 (2010).